Accepted manuscript by PCCP. Unformatted. Recompiled: May 17, 2017

Novel High-Temperature Ferroelectric Domain Morphology in $PbTiO_3$ Ultrathin Films

J. B. J. Chapman,[1,2] A. V. Kimmel,[2,1] and D. M. Duffy[1]

[1] *Department of Physics and Astronomy, University College London, Gower Street, London WC1E 6BT, UK*
[2] *National Physical Laboratory, Hampton Road, Teddington, TW11 0LW, UK*

(Dated: May 17, 2017)

Exotic domain morphologies in ferroic materials are an exciting avenue for the development of novel nanoelectronics. In this work we have used large scale molecular dynamics to construct a strain-temperature phase diagram of the domain morphology of $PbTiO_3$ ultrathin films. Sampling a wide interval of strain values over a temperature range up to the Curie temperature T_c, we found that epitaxial strain induces the formation of a variety of closure- and in-plane domain morphologies. The local strain and ferroelectric-antiferrodistortive coupling at the film surface vary for the strain mediated transition sequence and this could offer a route for experimental observation of the morphologies. Remarkably, we identify a new nanobubble domain morphology that is stable in the high-temperature regime for compressively strained $PbTiO_3$. We demonstrate that the formation mechanism of the nanobubble domains morphology is related to the wandering of flux closure domain walls, which we characterise using the hypertoroidal moment. These results provide insight into the local behaviour and dynamics of ferroelectric domains in ultrathin films to open up potential applications for bubble domains in new technologies and pathways to control and exploit novel phenomena in dimensionally constrained materials.

INTRODUCTION

Domain walls in thin films have shown promising functionalities, such as induced electric and magnetic properties, and the formation of unusual controllable phases that are not observed in the bulk samples [1–4]. Recent direct observation of so-called *wandering* domain walls in thin films [5], whereby the direction of the domain wall tangent significantly varies along the wall length, and the ability to control the direction of the domain wall suggests viable mechanisms for tuning intrinsic ferroelectric and piezoelectric properties [6, 7].

The orientation of the polarisation in ferroelectric films is influenced by a delicate balance between the epitaxial strain and screening of the depolarising field. The misfit strain from growth substrates has been shown to promote exotic polar orientations that are not observed in bulk samples [8, 9]. Similarly, compensation of the intrinsic depolarising field through screening has been shown to induce the formation of novel ordered domain structures [10]. A rich variety of new closure domain morphologies, such as Landau-Lifshitz stripe domains [11, 12], vortex and triclinic domains [13], have been predicted in $PbTiO_3$, and $BaTiO_3$ thin films under open-circuit boundary conditions using density functional theory, effective Hamiltonian and interatomic potential models[14, 15]. Tantalising experimental evidence for these closure domains in platlets and dots of $BaTiO_3$ has been presented in the form of 90° stripe superdomains bifurcated by 180° domain walls[16–18] and recent direct observation of vortices in $PbTiO_3/SrTiO_3$ superlattices[19].

The insight into the atomistic mechanisms of formation of dense domain morphologies is fundamentally and industrially important for the next generation of emergent technologies. Density functional theory (DFT) calculations have been extensively applied to various ferroelectric materials and these have provided fundamental insight into the origin of ferroelectricity, domain wall behaviour, grain boundaries and interfacial phenomena [20–23]. However, modelling of domain wall dynamics at DFT level is computationally challenging since this requires large ensembles and long computation times. Semi-empirical forcefields, parametrised to reproduce materials properties, provide robust tools for modelling long timescale dynamics and dense sampling of strain values.

In this paper we model domain morphologies formed in $PbTiO_3$ films using molecular dyanamics and calculate the misfit-strain – temperature (Pertsev diagram [8]) of symmetrically terminated $PbTiO_3$ films for a wide range of strain and temperature values. We identify the effect on the domain structure on the ferroelectric-antiferrodistortive coupling at the films surfaces and found that epitaxial strain induces the formation of a variety of closure- and in-plane domain morphologies. Remarkably, we identified a new nanobubble domain morphology that was stable in the high-temperature regime. We demonstrate that the formation mechanism of the novel nanobubble domain morphology is related to the wandering of flux closure domain walls.

METHODOLOGY

We studied (001) properties of strained $PbTiO_3$ ultrathin films under open circuit conditions using molecular dynamics as implemented in the DL_POLY code [24]. We used the adiabatic core-shell forcefield derived in Gindele et al., that reproduces the structural parameters of the cubic and tetragonal phases, the Born effective charge tensors, the elastic properties and soft phonon modes of $PbTiO_3$ in excellent agreement with density functional theory (DFT) calculations[25]. Furthermore, the model correctly describes the enhanced antiferrodistortive c(2x2) surface relaxation of $PbTiO_3$ in agreement with ab initio calculations [26, 27].

We use a large supercell of size 10x10x10 (z=10 layer PbO only) to create a symmetrically terminated film containing 4700 atoms (and larger in some cases, explicitly mentioned) with three dimensional periodic boundary conditions. A 100 Å vacuum gap in the growth direction $[001]_p$ was imposed on the system so the film is continuous and infinite along the pseudocubic $[100]_p$ and $[010]_p$ directions.The homogeneous biaxial misfit strain was defined as

$$\eta = \frac{a_s}{a_f} - 1 \tag{1}$$

where a_f is the cubic lattice parameter at the Curie temperature T_c. The properties of the system were calculated at different values of strain via variation of the effective substrate lattice parameters a_s in the range $3.8 < a_s < 4.05$ (Å). The misfit strain was imposed by a Nosé-Hoover canonical (NVT) ensemble with a 10 fs relaxation constant. For each misfit strain the system was heated over a temperature range of 25< T <1000 (K) in 25 K increments; equilibrated at each temperature for 20 ps using a 0.2 fs timestep, with statistics gathered over a subsequent 60 ps production run. To confirm the consistency of our results we repeated several calculations using random selections of misfit strains within a set of larger systems ($10 \leq N_{x,y} \leq 26$). We note a small variation (within 10%) of the temperature and strain values of phase changes with larger systems and attribute this to the competitive energy balance between an increase of the domain volume against the domain wall area.

The initial slab configuration was prepared to include two anti-aligned *out-of-plane* ideal Kittel domains with imposed ferroelectric displacements within each domain. To satisfy periodic boundary conditions the film contained two domain walls centred on the PbO(100) planes whose surface normal was parallel to the pseudocubic $[100]_p$ direction.

We define the effective local polarisation as the dipole per unit volume of a Ti centred conventional unit cell [$TiPb_8O_6$], delimited by 8 Pb cations with 6 oxygen on the trigonal faces forming a complete octahedral cage about the Ti cation[25]. The contributions from the dipoles separating all cores and shells in the cell are considered with reference to the Ti core site:

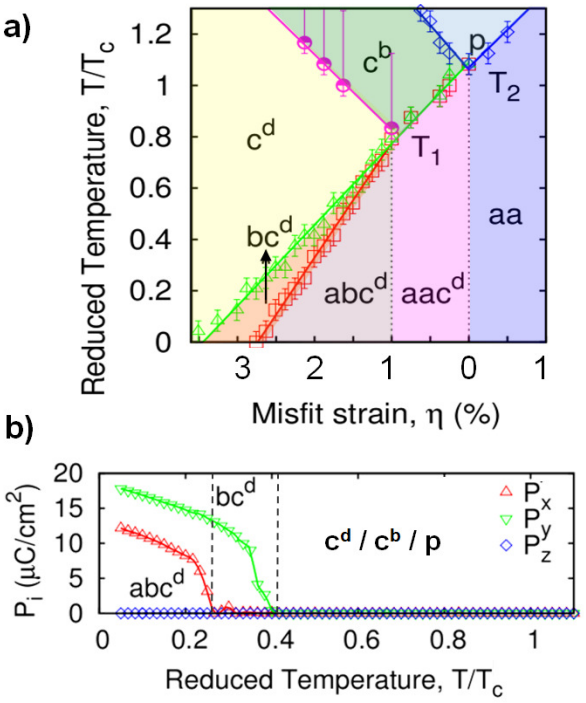

FIG. 1: Domain morphology dependence on misfit strain and temperature. (a) Pertsev diagram for 3.8 nm thick (001)$PbTiO_3$ calculated using the core-shell model. (b) Macroscopic polarisation dependence on temperature for η =-2.25%.

$$\vec{P}^j = \frac{1}{\nu^j} \sum_{i=1}^{29} \frac{1}{\omega^i} q^i (\vec{r}^{j,i} - \vec{r}^{j}) \tag{2}$$

where ν^j is the volume of the cell calculated via the local lattice vectors, $\vec{r}^{j,i}$ is the position vector of the i^{th} particle in the j^{th} unit cell with respect to the supercell origin, q^i is the charge of the i^{th} particle species and ω^i is a weight to normalise the charge of the i^{th} particle with respect to the number of cells it is shared amongst.

RESULTS AND DISCUSSION

Figure 1a presents the results of the observed domain morphologies over the full temperature and strain range considered. Our results are in excellent agreement with observations from other theoretical methods[6, 28] so we adopt the nomenclature of Jiang et al. whereby a,b,c label principle axes along which the polarisation is finite. A superscript d indicates the out-of-plane polarisation is in the form of periodic domains. The definition of each phase in relation to behaviour of the local and macroscopic polarisation is summarised in Table I and characterised from the polarisation profile which is shown

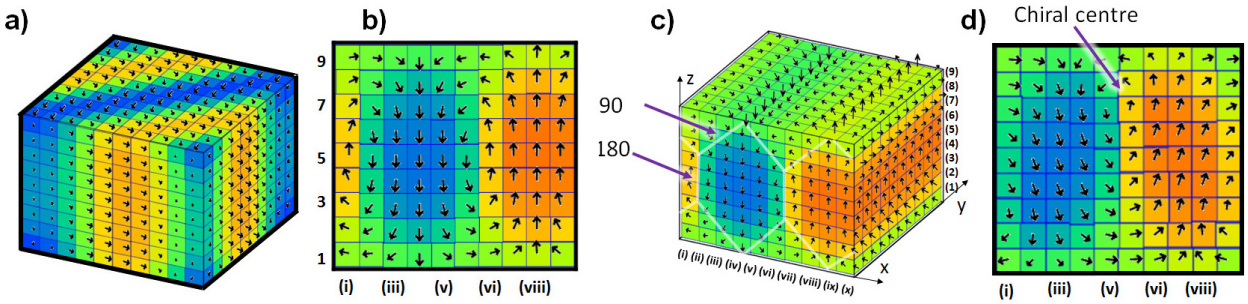

FIG. 2: Domain morphologies of $PbTiO_3$ ultrathin films. Each unit cell is represented by a cube coloured proportional to the polarisation. TiO_2 stack layers index the (001) TiO_2 planes defined from the film base. Bracketed numerals define (100) columns of unit cells along $\hat{x}$. (a) Perspective view of the **aa** domains. (b) x-z cross-section of the film with the $\mathbf{c^d}$ domain morphology. (c) Perspective view of the $\mathbf{c^d}$ domains. (d) x-z cross-section of the film with the $\mathbf{abc^d}$ domain patterning.

TABLE I: Morphological definitions based on microscopic polarisations of each local unit cell P_k^j and the overall macroscopic polarisation $P_k = \sum_j P_k^j/N$. $P_z^j \neq 0$ is the criterion that the local out-of-plane polarisation can be non-zero, but due to the depolarising field $P_z = 0$ for all cases necessary from the open-circuit boundary conditions. The local polarisation criteria are not applied to the surface and 1st subsurface layers due to surface relaxations. (†) wandering domain walls which converge to produce $\mathbf{c^b}$ domains.

Domain	Total Polarisation	Local Polarisation
$\mathbf{c^d}$	$P_x = P_y = P_z = 0$	$P_z^j \neq 0$
$\mathbf{bc^d}$	$P_x = P_z = 0, P_y \neq 0$	$P_z^j \neq 0$
$\mathbf{abc^d}$	$P_x \neq P_y \neq 0, P_z = 0$	$P_z^j \neq 0$
$\mathbf{aac^d}$	$P_x = P_y \neq 0, P_z = 0$	$P_z^j \neq 0$
aa	$P_x = P_y \neq 0, P_z = 0$	$P_z^j = 0$
p	$P_x = P_y = P_z = 0$	$P_z^j = 0$
(†)	$P_x = P_y = P_z = 0$	$P_z^j \neq 0$, $P(x,y,z) \neq P(x,y',z)$

in Figure 1b for $\eta = -2.25\%$. We observe three distinct ferroelectric domain morphologies: **aa**, $\mathbf{c^d}$ and $\mathbf{abc^d}$ (shown in Figure 2, of which we henceforth loosely refer to as phases). Between these distinct phases we find two strain induced transitional ferroelectric phases $\mathbf{bc^d}$ and $\mathbf{aac^d}$. A paraelectric phase **p** exists for all phases above the Curie temperature $T_c(\eta)$. Remarkably, in addition to the three distinct phases, we have identified a fourth previously unreported misfit-strain domain phase at high temperatures which we refer to as nanobubble domains $\mathbf{c^b}$.

aa Domains

Under tensile strain ($\eta > 0$) below the paraelectric transition temperature, with corresponding substrate lattice parameters $a_s > a_0$, the polarisation is oriented parallel to the substrate interface [29, 30]. Domains form with ordered regions polarised along the a and b principle axes separated via 90° domain walls (Figure 2a). As the magnitude of the polarisation in each domain is equivalent the domains are classified as **aa** and are similar to those presented by Kouser et al. using a model Hamiltonian [28].

$\mathbf{c^d}$ domains

Under compressive strain ($\eta < 0$) we observe the formation of closure domains that consist of periodic 180° out-of-plane stripe domains $\mathbf{c^d}$ (Figure 2b-c). This is consistent with experimental XRD results for $PbTiO_3$ films of similar thickness [31, 32] and $PbTiO_3/SrTiO_3$ superlattices [19, 33, 34]. Morphologically, these are *Landau-Lifshitz* domains having 90° closure domain *caps* at the surface as previously observed in theoretical studies of $PbTiO_3$ films using interatomic potentials[11, 35].

A film thickness dependence has previously been identified by Belletti et al. for the $\mathbf{c^d}$ phase showing the 180° domain walls (see Figure 2c) to vanish into a vertex as the film thickness is decreased[11]. Our simulations reproduce this dependence which further validates our model. By comparing the configurational energy per unit cell when increasing the supercell dimensions and film thickness (N_z), we further demonstrate our model satisfies the Kittel scaling law, obeying a linear dependence between the optimal domain width and the square root of the thickness. For films using $a_s = 3.99$ Å at 25 K the law is satisfied for $N_z \geq 5$ (001)PbO layers (2 nm) which returns a periodicity of 4.0 nm in agreement with experiment [31]. For thinner films the out-of-plane components of polarisation vanishes [32] but we observe that ferroelectricity is maintained with the polarisation reorientated in-plane (**a**-domain). Such reorientation has also been shown for $PbTiO_3$ films using DFT[36].

$\mathbf{abc^d}$ and Transitional Domain Morphologies ($\mathbf{bc^d}$ and $\mathbf{aac^d}$)

Under sequentially decreased compressive strains, components of polarisation can condense first parallel to the domain walls and then parallel to the domain periodicity (Figure 1) forming $\mathbf{bc^d}$, $\mathbf{abc^d}$ and finally $\mathbf{aac^d}$ domains through second order transitions. For each of these domains, out-of-plane stripe domains persist with the additional components superimposed. The x-z profile of the $\mathbf{bc^d}$ is identical to that of the $\mathbf{c^d}$ (Figure 2b).

For compressive strains between $1< \eta <3.75$ (%) the P_x component also condenses forming $\mathbf{abc^d}$ domains (Figure 2d). The symmetry breaking between the P_x and P_y critical temperatures (Figure 1b) occurs due to the requirement for dipoles to reorientate to form the closure domains parallel to the direction of domain periodicity [6, 28]. Our simulations show that the 180° domain walls of the adjacent $\mathbf{bc}^d$ phase collapse into to a vertex creating infinitely long cylindrical *chiral tubes*[37] as the polarisation parallel to the domain periodicity (P_x) stabilises further reducing the symmetry. This is consistent with observations in theoretical studies on PZT films[37]. Further to previous investigations, we observe that these chiral tubes propagate towards the film surface as the epitaxial compression is reduced further.

Our model shows a critical misfit strain of 1% upon which the chiral tubes reach the surfaces of the film and *dissipate*, equalizing the macroscopic in-plane polarisation components whilst maintaining distinct out-of-plane stripe domains, $\mathbf{aac^d}$ domains. The $\mathbf{aac^d}$ domains have a similar cross-section to the $\mathbf{abc^d}$ domains in Figure 2d with the quantitative exception $P_x = P_y$ and the loss of the chiral centres such that there is no remnant of the 90° domain caps (as weakly exists for the $\mathbf{abc^d}$ domains observable in Figure 2d above the chiral centre pointer). For compressive strains in the range $0 < \eta < 1$ (%) the magnitude of P_z in the $\mathbf{aac^d}$ domains reduce continuously to a limiting vanishing point of freestanding films upon which the **aa** domain pattern is recovered. Second order transitions of the polarisation by means of continuous dipole rotation with the local structure transitioning through low symmetry triclinic phases such as we observe have similarly been been identified in an effective Hamiltonian simulation on PZT subjected to variations in the depolarising field strength [10].

Dielectric Response

To reduce the error in our domain transition temperatures we evaluate the characteristic dielectric response of the films as it is known that susceptibility of ferroelectrics exhibits a divergent Curie-Weiss behaviour at the phase transition temperature. The susceptibility $\chi_{\alpha\beta}$ and dielectric $\epsilon_{\alpha\beta}$ tensors are calculated from fluctuations in the total polarisation[38, 39]:

$$\chi_{\alpha\beta} = \frac{\langle V \rangle}{\epsilon_0 k_B T}(\langle \vec{P}_\alpha \cdot \vec{P}_\beta \rangle - \langle \vec{P}_\alpha \rangle \cdot \langle \vec{P}_\beta \rangle) \qquad (3)$$

where k_B, T and ϵ_0 are the Boltzmann constant, simulation temperature and permittivity of free-space, respectively and $\langle V \rangle$ is the time-averaged volume of the film. α and β correspond components of the basis vector having labels of x, y or z which define the tensor element. The bulk high-frequency (optical) susceptibility χ_∞ for $PbTiO_3$ is 8.24 and, therefore, negligible in relation to the static component [40].

We find that both the $\mathbf{c^b} \rightarrow \mathbf{bc^d}$ and $\mathbf{bc^d} \rightarrow \mathbf{abc^d}$ transitions are accompanied by large dielectric response. Indeed, Figure 3 shows asymptotic behaviour for χ_{xx} and χ_{yy} corresponding to the condensation of P_x and P_y components, respectively.

The transition temperature between the domain phases are then determined from the linear high temperature dependence of the inverse dielectric constant ϵ^{-1} (Figure 3-inset). For $\eta = -2.26\%$ shown in Figure 3, the transition temperatures from the extrapolation are $0.27T_c$ and $0.36T_c$ for the $\mathbf{bc^d} \rightarrow \mathbf{abc^d}$ and $\mathbf{c^d} \rightarrow \mathbf{bc^d}$ transitions, respectively, with an uncertainty of ±4.4%. Our studies are performed for the system under open circuit electrical boundary conditions which results in the presence of a strong depolarising field. The latter prevents the formation of an out-of-plane dielectric response ($\epsilon_{zz} = 0$). A corresponding increase in χ_{zz} would be expected for imperfect screening approaching the Curie temperature[28].

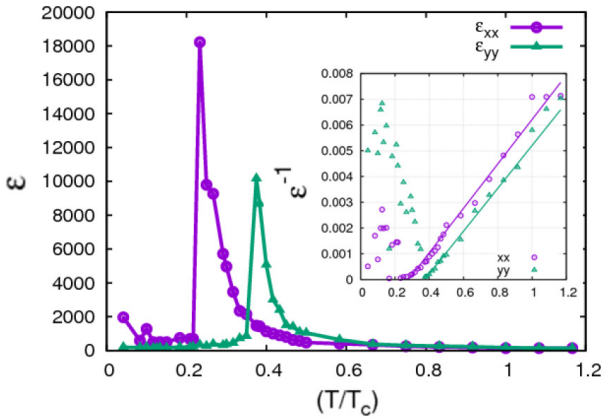

FIG. 3: Temperature dependence of the static dielectric constant of a $PbTiO_3$ film for $\eta = -2.26\%$ identifying transition to different ferroelectric domains. A divergent response is observed for the $\mathbf{c^b} \rightarrow \mathbf{bc^d}$ transition (ϵ_{yy}) and $\mathbf{bc^d} \rightarrow \mathbf{abc^d}$ (ϵ_{xx}) transitions. Inset: Inverse dielectric constant with linear extrapolation from the high temperature response providing a more accurate estimation of the domain *phase* transition temperatures.

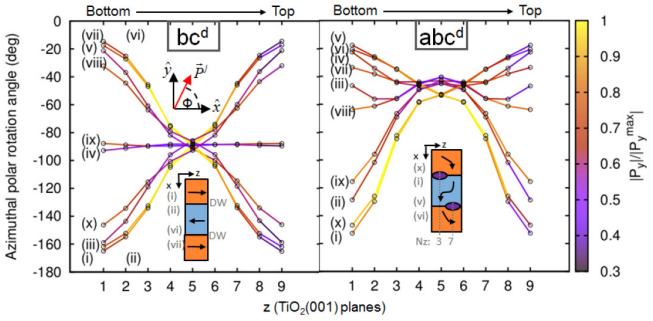

FIG. 4: (Color online). In-plane polarisation angle ($\phi = \tan^{-1}(P_y/P_x)$) and relative intensity of local polarisation chains in different $PbTiO_3$ domain morphologies confirming the domain wall in $\mathbf{bc}^d$ and chiral centre in $\mathbf{abc}^d$ domains are vortex centres in films. Bracketed Roman numerals index the unit cell column relative to the domain walls as defined in Figure 2. TiO_2 stack layers 1 and 9 are the rows of unit cells on the bottom and top surfaces, respectively. $[010]_p$ polarisation maximised through 180° domain walls and the chiral centres.

Novel Properties of $\mathbf{bc}^{\mathbf{d}}$ and $\mathbf{abc}^{\mathbf{d}}$ Domains

Theoretical studies have previously shown $PbTiO_3$ films to have different critical temperatures of the in-plane components of macroscopic polarisation [6, 28]. This results in the $\mathbf{abc}^{\mathbf{d}} \rightarrow \mathbf{bc}^{\mathbf{d}} \rightarrow \mathbf{c}^{\mathbf{d}}$ transition sequence under the compressive strain regime, but knowledge of the behaviour of the local polarisation within each domain remains limited. To address the lack of knowledge about the polar behaviour with domain morphology we have analysed the in-plane components of polarisation within each of the closure domain morphologies ($\eta < 0$) at $\eta = -2.15\%$.

In the $\mathbf{bc}^{\mathbf{d}}$ domain phase, our simulations reveal the in-plane dipole rotations are not homogeneous throughout the film. The P_y component (perpendicular to both the domain wall and surface normals), has a maximum value within unit cells constituting the domain walls (cell stacks (i), (ii), (vi) and (vii) in Figure 4a) and reduces sharply for cells further from the domain wall, reorientating along the *c*-axis at the centre of the film away from surface effects. The polar rotations at the surface layers act to change the anisotropy, forcing the domain walls to be more characteristic of magnetic Bloch-Néel walls than the distinctly Ising form in bulk [41]. Evidence for the existence of mixed Ising and Bloch-Néel character domain walls in ferroelectrics has recently been proposed in $PbTiO_3$ and $LiNbO_3$ from *ab initio* calculations [42]. Such dipolar rotations can cause band bending of the conduction states across the domain wall and may be a contributory cause for recent experimental observations of conductive domain walls [43].

We further identify the P_y component of local polarisation in the $\mathbf{abc}^{\mathbf{d}}$ domains have a maximum magnitude about the chiral centres producing concentric tubes of increasing in-plane ferroelectricity (Figure 4b). The $\mathbf{c}^{\mathbf{d}}$ domains exhibit no macroscopic or local polarisation parallel to $[010]_p$, only supporting rotations tangent to the $(010)_p$ plane which are required to close flux at surface layers.

The coupling between antiferrodistortive (AFD) rotations and the local dipole moments are rarely investigated, yet such interactions have been shown to influence Curie temperatures and phases that can produce improper ferroelectrics [12, 44]. It has recently been proposed that control of AFD chiralities could be used in novel technologies such as four-state memory making the identity of methods to control AFD behaviour at atomic scales paramount [45]. Here, we demonstrate the effects of ferroelectric-antiferrodistortive coupling between the c(2x2) AFD surface reconstruction and the ferroelectric (FE) closure domain patterns at the surface of the $PbTiO_3$ film[26, 27]. This is characterised by the rotation of the equatorial oxygen atoms about the titanium, with simultaneous out-of-plane distortions which vary along the direction of the domain wall normals $[001]_p$. The TiO_6 octahedral rotations are averaged over the full trajectory and through $[010]_p$, and are presented in Figure 5a for the $\mathbf{c}^{\mathbf{d}}$, $\mathbf{bc}^{\mathbf{d}}$ and $\mathbf{abc}^{\mathbf{d}}$ domain configurations along both the surfaces.

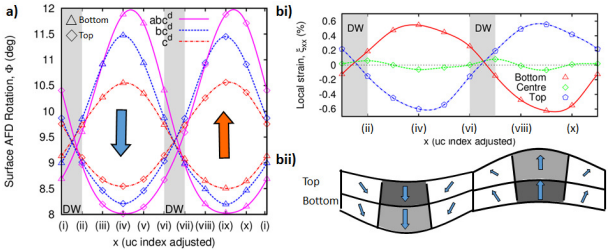

FIG. 5: FE-AFD coupling on the surface of a 3.8 nm thick $PbTiO_3$ ultrathin film with different ferroelectric closure domain configurations. (a) Rotation angle (Φ) on the top (diamond) and bottom (triangle) surfaces for each closure domain configuration. The arrows represent the out-of-plane domain orientation. (bi) Local strain along the top surface (pentagon), bottom surface (triangle) and centre (diamond) of the film with the $\mathbf{c}^{\mathbf{d}}$ domain morphology. (bii) Cartoon illustrating the local strain dependence on polarisation orientation at the top and bottom surface.

For the $\mathbf{c}^{\mathbf{d}}$ domains a sinusoidal dependence is noted with a maximum rotation at the centre of the domain when the polarisation is pointing out-of-plane and minimised when the polarisation points into the plane (Figure 5a). Due to the symmetry of the domain pattern, the profiles of the rotation angle Φ for the top and bottom surface are identical, albeit inverted for any given point along $[100]_p$. The same relation has previously been noted for films with a $\mathbf{c}^{\mathbf{d}}$ domain configuration modelled using a shell model which sampled three points along

$[100]_p$[11]. The angle variations for the other domain phases have not previously been reported, nor has direct explanation for the mechanism changing the rotation angle.

For both $\mathbf{bc^d}$ and $\mathbf{abc^d}$ the maxima and minima occur at the centre of the domains for the polarisation pointing out and in, respectively, although there is a slight shift in the absolute position along $[100]_p$ in the case of the $\mathbf{abc^d}$ domain due to change from 180° domain walls to chiral centres moving from the film centre (Figure 2d). However, due to the change of symmetry of the domain patterns, at a given point along $[100]_p$ the top and bottom of the film no longer share inversion symmetry, breaking this relationship in the Φ profile. Further, the magnitude of the rotation increases upon transition into the successive domain phases ($\mathbf{c^d}$(red) → $\mathbf{bc^d}$ (blue) → $\mathbf{abc^d}$ (purple)).

A DFT study into the AFD modes of bulk $PbTiO_3$ has previously shown a direct strain dependence on the rotation angle, showing for strains larger than a critical value, the angle increases with tensile strain [46]. We show the local strain profile of a chain of unit cells along $[100]_p$ at the top, bottom and centre of the film in Figure 5b for the $\mathbf{c^d}$ phase. Comparison of the strain-profile to Figure 5a(red) shows a clear relationship between local strain and Φ, as is observed in bulk. Increases in local tensile strain enhance the rotation angle, whereas compressive strains suppress the rotation. A cartoon depicting the top and bottom surfaces is shown in Figure 5b(ii) demonstrating the strain-polarisation coupling acting as the mechanism promoting the variation in rotation angle. The transition from $\mathbf{c^d} \rightarrow \mathbf{bc^d} \rightarrow \mathbf{abc^d}$ occurs with positive increases in strain (at a fixed temperature, Figure 1a) revealing the cause for the increase in rotation angle with the domain phase sequence.

New High Temperature Nanobubble Domain Morphology

In addition to the previously predicted phases, our model finds an entirely new phase at temperatures above the $\mathbf{c^d}$ phase but below T_c. Our simulations show that in the compressive strain regime, in the vicinity of the effective Curie temperature, the homogeneity of the stripe $\mathbf{c^d}$ domains along the easy axis, the in-plane $[010]_p$ direction, breaks down. This is due to diffuse nucleation and growth of the reverse domain on the domain walls (Figure 6a), shown previously as a growth mechanism in bulk prototypical systems under an activation field using a Landau-Ginzburg-Devonshire model [47]. This first presents by the distortion of the 180° domain wall alignment with $(100)_p$ planes (Figure 6a-d), so-called '*wandering*' [5, 6]. Here we observed that, with further temperature increases leading to polarisation reduction, the degree of the anisotropy increases resulting in the domain wall pattern changing from linear stripe domains into *nanobubble domains* (Figure 6e). To confirm the prediction of this domain pattern, films of the same thickness were modelled using a larger simulation cell. Constructing the film using $26 \times 26 \times 10$ unit cells, the $\mathbf{c^b}$ domains were shown to persist, forming through the same mechanism and therefore not a consequence of the chosen supercell size (Figure 6 f-g).

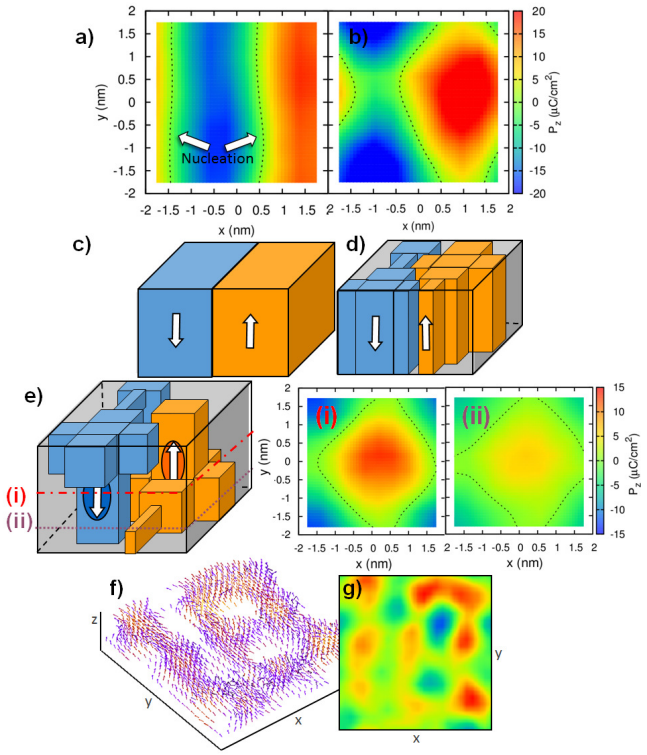

FIG. 6: New ferroelectric domain morphology - nanobubble domains $\mathbf{c^b}$. Out-of-plane polarisation profile at the centre (N_z=5) of the $PbTiO_3$ film for (a) 180° domain wall along easy axis (b) wandering 180° domain wall. (c,d) Cartoons depicting the 180° domain wall structures near film centre. (e) Cartoon of the predicted $\mathbf{c^b}$ domain. Out-of-plane polarisation profiles from unit cells on the N_z=5 (i) and N_z=2 (ii) (001) planes of a $10 \times 10 \times 10$ simulation cell. Dotted lines define the interpolated $P_z = 0$ isoline. (f) Large scale simulation showing the local dipoles of $\mathbf{c^b}$ domains in compressively strained $PbTiO_3$ calculated using a $26 \times 26 \times 10$ cell containing 31772 atoms - for clarity only local dipoles with $P_z^j > 0$ are plotted leaving voids where $P_z^j < 0$. (g) Out-of-plane polarisation contour map of the centre (001) plane of (f) - red $P_z > 0$, blue $P_z < 0$.

The tendency for domain walls to wander emerges from the T_1 multiphase point in the Pertsev diagram increasing linearly with compression (Figure 1a). Once established, the nanobubble domains are shown to persist until $T_c(\eta)$. Similar arrays of nanoscale bubble domains have been predicted in PZT on the transition path between Landau-Lifshitz domains to a monodomain under an applied electric field at 10 K [10]. To our knowledge, these domains

have not previously been identified in pure $PbTiO_3$ or for the condition of open circuit boundaries. The faceting instabilities of the nanobubble domains (Figure 6e-f) are analogous to those that occur from surface tension instabilities in thin magnetic films [48].

The presence of nanobubble domains is generally difficult to detect as there is no change to the total polarisation (Figure 1b), nor is there an accompanied dielectric response (Figure 3). To address this difficulty a new order parameter, the hypertoroidal moment $\vec{h}$, was proposed[49]:

$$\vec{h} = \frac{1}{2V}\sum_j \vec{r}^j \times \vec{T}_t^j = \frac{1}{4V}\sum_j \vec{r}^j \times (\vec{r}^j \times \vec{P}_t^j)_t \qquad (4)$$

where the index j spans all unit cells, V is the supercell volume and $\vec{r}^j$ is the position vector of the j^{th} unit cell relative to a chosen origin with coordinates transformed to set the origin at the centre of the supercell. $\vec{T}_t^j$ and $\vec{P}_t^j$ are the transverse components of the local toroidal and dipole moments where we make the approximation $\vec{P}_t^j \approx \vec{P}^j - \langle\vec{P}\rangle$ using the time averaged total polarisation $\langle\vec{P}\rangle$.

Unlike the toroidal moment $\vec{T}$, which is physically interpreted as the average curl of the polarisation field, the hypertoroidal moment describes the average curl of the toroidal field. Therefore, it does not vanish for symmetries of twinned vortices such as the Landau-Lifshitz closure domains and yet it is sensitive to microscopic changes in polar ordering. Since $\vec{h}$ is multivalued for dimensionally constrained systems, dependent upon the choice of origin used to mimic the periodic supercell, we sample the surface of $\vec{h}$ for a set of supercells centred on coordinates corresponding to an xy scan of the central $(001)_p$ plane of the film. A similar procedure was first used to investigate the surface of the hypertoroidal moment for $PbTiO_3$ thin films with Landau-Lifshitz domains, switching due to strain gradients[11], where a sinusoidal dependence in h_z for the $\mathbf{c^d}$ domain configuration was shown as is found here (Figure 7a). Similarly, the turning points along $[100]_p$ correspond to the centres of the domains ($h_z(centre) = \pm|h_{z,max}|$) and the domain walls ($h_z(DW) = 0$) and therefore they have the same period as the underlying domain configuration.

For PZT films under an short circuit boundary conditions, the transition from closure domains to monodomains via nanobubble domains has been shown to correspond to an accompanying divergence in the hypertoroidal moment susceptibility[49] but the hypertoroidal moment surface for the domain morphology has not previously been characterised. Here, for the first time, we show the hypertoroidal moment surface for nanobubble ($\mathbf{c^b}$) domains (Figure 7b). The bubble domain cores correspond to the maxima (for the positively poled nanobubble) and minima (for the negatively poled nanobubble) in the surface of h_z. The origins of the hypertoroidal supercell corresponding to a vanishing moment agree with the $P_z = 0$ isoline in Figure 6e(i). As such we conclude the contours of the surfaces (a & b) show the hypertoroidal moment capable of characterising the polarisation distribution (Figure 6), supporting its proposed use as a suitable order parameter when the total polarisation remains unchanged.

Due to the domain transitions, wall wandering and multivalued property of $\vec{h}$, a common origin for the supercell used to mimic the periodic system cannot be defined. Therefore, to gain further insight into the temperature dependence, cross sections at $y_h = 0$ (see dashed line in Figure 7) are taken of the hypertoroidal moments surface at regular temperature intervals in Figure 7. The sinusoidal dependence of $\mathbf{c^d}$ is clearly evident at $0.167T_c$ but deformations to the sine wave are evident above $0.5T_c$, which is lower than the temperature at which deformations in the domain walls can start to be observed in the polarisation map (Figure 6a, $0.8T_c$). To guide the eye to these subtle deformations, a sinusoid (dotted) has been fitted to the h_z surface cross-sections. We assert that the kinks are evidence of small statistical variations in the polarisation from the 180° walls into the domains, which lead to the wandering domain wall phenomenon.

CONCLUSIONS

In this paper we have calculated the domain morphologies which condensate under varying homogeneous strains and temperatures within ultrathin films of $PbTiO_3$ using molecular dynamics with a shell model interatomic potential. We investigated the local behaviour of polarisation with the domains and identified a previously unreported high temperature nanobubble domain pattern. We have found that, in the vicinity of the Curie temperature, the 180° domain walls wander from the easy axis, leading to the formation of this new domain morphology. We characterised the nanobubble domains using the hypertoroidal moment surface (h_z) for the first time and showed that it can be used to identify minute changes in the polarisation profile which signalled the domain wall wandering. Ferroelectric-antiferrodistortive coupling was observed at the film surface. The rotation angle of the octahedral cages was determined to be dependent upon the local strain, increasing with tensile strain and consequently enhanced along the strain mediated transition sequence $\Phi_{max}(\mathbf{c^d}) < \Phi_{max}(\mathbf{bc^d}) < \Phi_{max}(\mathbf{abc^d})$. Such surface properties provide a alternative means for experimental verification of the underlying domain structures.

In summary, the results from the forcefield calculations give unprecedented details about the response of the local polarization in ultrathin ferroelectric films to variations in strain and temperature, leading to the identification of a novel high temperature nanobubble domain pattern. Our studies provide guidance for the application of strain

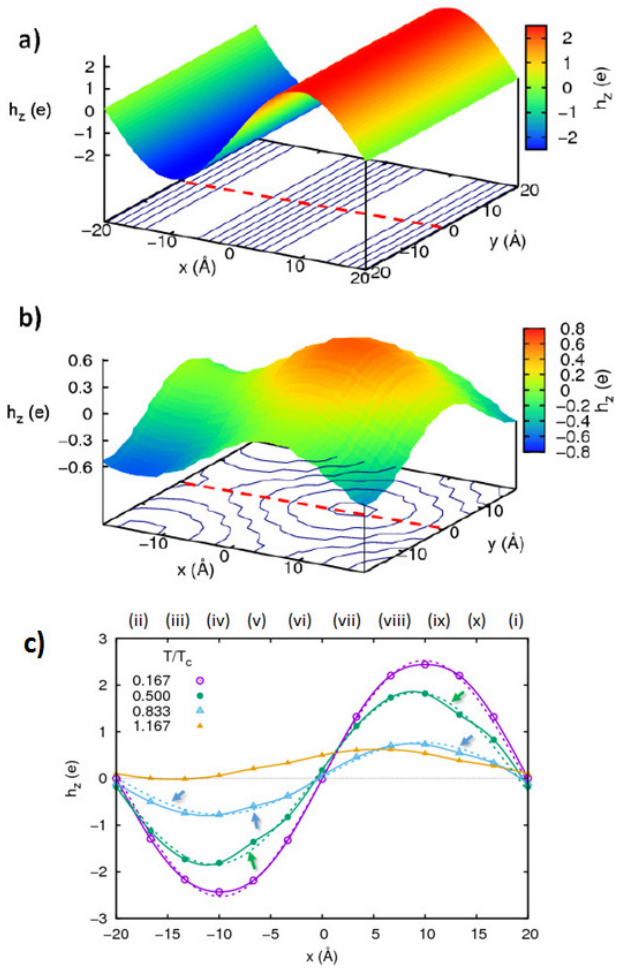

FIG. 7: Surface of the out-of-plane component of the hypertoroidal moment (h_z) evaluated the central (001) plane of the $PbTiO_3$ ultrathin film for (a) $\mathbf{c^d}$ domain configuration (b) $\mathbf{c^b}$ domain configuration. (c) Cross section of the out-of-plane component of the hypertoroidal moment surface evaluated for domain configurations as a function of temperature. Data points correspond to supercell origins which centre on titanium coordinates in the simulation cell. The dotted lines are sinusoids of the form $h(x) = A\sin(2\pi x/L_x + \phi)$ fit by method of least squares to the h_z-surface cross-sections of the closure-domains. Arrows show kinks in the surface.

engineering to ultra-dense domain pattern construction.

ACKNOWLEDGEMENTS

The authors thank Dr. Pavlo Zubko, Prof. J. Marty Gregg and Dr. Alina Schilling for fruitful discussions. Funding was provided by the EPSRC (EP/G036675/1) via the Centre for Doctoral Training in Molecular Modelling and Materials Science at University College London and the National Measurement Office of the UK Department of Business Innovation and Skills. Computer services on Archer were provided via membership of the UK's HPC Materials Chemistry Consortium funded by EPSRC (EP/L000202). We acknowledge the use of the UCL facilities LEGION and GRACE, and computational resources at the London Centre for Nanotechnology.

[1] S. Farokhipoor, C. Magen, S. Venkatesan, J. Iniguez, C. J. M. Daumont, D. Rubi, E. Snoeck, M. Mostovoy, C. de Graaf, A. Muller, et al., Nature **515**, 379 (2014).
[2] M. Daraktchiev, G. Catalan, and J. F. Scott, Physical Review B **81**, 224118 (2010).
[3] J. Seidel, L. W. Martin, Q. He, Q. Zhan, Y. H. Chu, A. Rother, M. E. Hawkridge, P. Maksymovych, P. Yu, M. Gajek, et al., Nature **8**, 229 (2009).
[4] D. Meier, J. Seidel, A. Cano, K. Delaney, Y. Kurnagai, M. Mostovoy, N. A. Spaldin, R. Ramesh, and M. Fiebig, Nature **11**, 284 (2012).
[5] C. L. Jia, K. W. Urban, M. Alexe, D. Hesse, and I. Vrejoiu, Science **331**, 1420 (2011).
[6] Z. J. Jiang, R. Z. Zhang, D. W. Wang, D. Sichuga, C. L. Jia, and L. Belliache, Physical Review B **89**, 214113 (2014).
[7] D. G. Schlom, L. Q. Chen, C. B. Eom, K. M. Rabe, S. K. Streiffer, and J. M. Triscone, Annual Review of Materials Research **37**, 589 (2007).
[8] N. A. Pertsev, A. G. Zembilgotov, and A. K. Tagantsev, Physical Review Letters **80**, 1988 (1998).
[9] N. A. Pertsev, A. K. Tagantsev, and N. Setter, Physical Review B **61**, R825 (2000).
[10] I. Kornev, H. X. Fu, and L. Bellaiche, Physical Review Letters **93**, 196104 (2004).
[11] G. D. Belletti, S. D. Dalosto, and S. Tinte, Physical Review B **89**, 174104 (2014).
[12] D. Sichuga, I. Ponomareva, and L. Bellaiche, Physical Review B **80**, 134116 (2009).
[13] I. I. Naumov, L. Bellaiche, and H. X. Fu, Nature **432**, 737 (2004).
[14] T. Shimada, S. Tomoda, and T. Kitamura, Physical Review B **81**, 144116 (2010).
[15] A. R. Balakrishna and J. E. Huber, Applied Physics Letters **106**, 092906 (2015).
[16] A. Schilling, D. Byrne, G. Catalan, K. G. Webber, Y. A. Genenko, G. S. Wu, J. F. Scott, and J. M. Gregg, Nano Letters **9**, 3359 (2009).
[17] R. G. P. McQuaid, L. J. McGilly, P. Sharma, A. Gruverman, and J. M. Gregg, Nature Communications **2**, 404 (2011).
[18] L. J. McGilly and J. M. Gregg, Nano Letters **11**, 4490 (2011).
[19] A. K. Yadav, C. T. Nelson, S. L. Hsu, Z. Hong, J. D. Clarkson, S. C. M, A. R. Damodaran, P. Shafer, E. Arenholz, L. R. Dedon, et al., Nature **530**, 198 (2016).
[20] D. Vanderbilt, Current Opinion in Solid State and Materials Science **2**, 701 (1997).
[21] K. M. Rabe and P. Ghosez, Topics in Applied Physics **105**, 117 (2007).
[22] P. Marton, T. Shimada, T. Kitamura, and C. Elsässer, Physical Review B **83**, 064110 (2011).
[23] X. Liu, Y. Wang, P. V. Lukashev, J. D. Burton, and E. Y. Tsymbal, Physical Review B **85**, 125407 (2012).

[24] I. T. Todorov, W. Smith, K. Trachenko, and M. T. Dove, Journal of Materials Chemistry **16**, 1911 (2006).
[25] O. Gindele, A. Kimmel, M. G. Cain, and D. Duffy, Journal of Physical Chemistry C **119**, 17784 (2015).
[26] A. Munkholm, S. K. Streiffer, M. V. R. Murty, J. A. Eastman, C. Thompson, O. Auciello, L. Thompson, J. F. Moore, and G. B. Stephenson, Physical Review Letters **88**, 016101 (2002).
[27] C. Bungaro and K. M. Rabe, Physical Review B **71**, 035420 (2005).
[28] S. Kouser, T. Nishimatsu, and U. V. Waghmare, Physical Review B **88**, 064102 (2013).
[29] O. Dieguez, K. M. Rabe, and D. Vanderbilt, Physical Review B **72**, 144101 (2005).
[30] R. D. Kingsmith and D. Vanderbilt, Physical Review B **49**, 5828 (1994).
[31] S. K. Streiffer, J. A. Eastman, D. D. Fong, C. Thompson, A. Munkholm, M. V. R. Murty, O. Auciello, G. R. Bai, and G. B. Stephenson, Physical Review Letters **89**, 067601 (2002).
[32] D. D. Fong, G. B. Stephenson, S. K. Streiffer, J. A. Eastman, O. Auciello, P. H. Fuoss, and C. Thompson, Science **304**, 1650 (2004).
[33] P. Zubko, N. Jecklin, N. Stucki, C. Lichtensteiger, G. Rispens, and J.-M. Trisone, Ferroelectrics **433**, 127 (2012).
[34] P. Aguando-Puente and J. Junquera, Physical Review B **85**, 184105 (2012).
[35] M. G. Stachiotti and M. Sepliarsky, Physical Review Letters **106**, 137601 (2011).
[36] B. K. Lai, I. Ponomareva, I. Kornev, L. Bellaiche, and G. Salamo, Applied Physics Letters **91**, 152909 (2007).
[37] D. Sichuga and L. Bellaiche, Physical Review Letters **106**, 196102 (2011).
[38] J. M. Caillol, D. Leveque, and J. J. Weis, Journal of Chemical Physics **85**, 6645 (1986).
[39] I. Ponomareva, L. Bellaiche, T. Ostapchuk, J. Hlinka, and P. J, Physical Review B **77**, 012102 (2008).
[40] P. Ghosez, E. Cockayne, U. V. Waghmare, and K. M. Rabe, Physical Review B **60**, 836 (1999).
[41] B. Meyer and D. Vanderbilt, Physical Review B **65**, 104111 (2002).
[42] D. Lee, R. Behera, P. P. Wu, H. X. Xu, S. B. Li, Y. L. Sinnott, S. R. Phillpot, L. Q. Chen, and V. Gopalan, Physical Review B **80**, 149904 (2009).
[43] S. Farokhipoor and B. Noheda, Physical Review Letters **107**, 127601 (2011).
[44] E. Bousquet, M. Dawber, N. Stucki, C. Lichtensteiger, P. Hermet, S. Gariglio, J.-M. Triscone, and P. Ghosez, Nature **452**, 732 (2008).
[45] D. Sichuga, W. Ren, S. Prosandeev, and L. Bellaiche, Physical Review Letters **104**, 207602 (2010).
[46] J. L. Blok, D. H. A. Blank, G. Rijnders, K. M. Rabe, and D. Vanderbilt, Physical Review B **84**, 205413 (2011).
[47] Y. H. Shin, I. Grinberg, I. W. Chen, and A. M. Rappe, Nature **449**, 881 (2007).
[48] A. A. Thiele, Journal of Applied Physics **41**, 1139 (1970).
[49] S. Prosandeev and L. Bellaiche, Journal of Materials Science **44**, 5235 (2009).